Research articles

Magnetic softness and magnetization dynamics of FeSiBNbCu(P,Mo) nanocrystalline alloys with good high-frequency characterization

Huiyun Xiao[a,b], Yaqiang Dong[a], Aina He[a,*], Hao Sun[a], Anding Wang[a,c,*], Hu Li[a], Lei Liu[a], Xincai Liu[b,*], Run-wei Li[a]

[a] CAS Key Laboratory of Magnetic Materials and Devices, Zhejiang Province Key Laboratory of Magnetic Materials and Application Technology, Ningbo Institute of Materials Technology and Engineering, Chinese Academy of Sciences, Ningbo, Zhejiang 315201, China
[b] School of Material Chemistry, Ningbo University, Ningbo, Zhejiang 315201, China
[c] Center for Advanced Structural Materials, Department of Mechanical and Biomedical Engineering, College of Science and Engineering, City University of Hong Kong, Kowloon, Hong Kong, China

ARTICLE INFO

ABSTRACT

In this study, the microalloying effects of P and Mo on thermal behavior, magnetic softness and magnetization process of FeSiBNbCu(P,Mo) nanocrystalline alloys were investigated systematically. The P and Mo bearing alloys exhibit pronouncedly improved magnetic softness, including extremely low coercivity of about 0.7 A/m, high saturation magnetic flux density of about 1.40 T, high permeability over 3.0×10^4 at 1 kHz. The excellent magnetic softness could be attributed to uniform dual-phase microstructure and wide strip magnetic domains after optimum annealing. The P and Mo containing alloys also have good high-frequency characterization, especially, the permeability at 100 kHz is still over 1.53×10^4. These alloys also have relatively low pinning field of 20–30 A/m, which means lesser defects and easier magnetization. Through observing the changes of magnetic domains and μ with applied field increasing, we found that the increase of μ is corresponding to reversible and irreversible movement of domain walls, after reaching the maximum, the decrease of μ is related to the rotation of magnetic moment and the split of domains.

1. Introduction

As soft magnetic functional materials, Fe-based nanocrystalline alloys with excellent magnetic softness containing quite low coercivity (H_c), low core loss (P), and high permeability (μ) [1–3], have been widely used in common mode chokes, inductors, high-frequency transformers, and other electrical devices. With the emergency of the global energy crisis and the progress of the science and technology, the development tendency of electrical devices is miniaturization, high efficiency and energy conservation [4]. This correspondingly desires Fe-based nanocrystalline alloys have higher saturation magnetization (B_s), lower P, higher μ, and better high-frequency stability than that of current alloys. Finemet nanocrystalline alloys not only have relatively low H_c and high μ, but also have been widely industrial used. However, the Finemet alloys also have two shortcomings which become increasingly obvious for low B_s of only 1.24 T and high material costs due to addition of 3 at.% precious element Nb [3,5,6]. By devoting subsequent great efforts, a variety of high B_s of FeZrB [7], (Fe$_{0.5}$Co$_{0.5}$)ZrB [8], FeSiBCCu [9], FeSiBCu [10], FeSiBPCu [11] and etc. were

successfully developed. Yet, these nanocrystalline alloys exhibit high H_c above 3 A/m, poor high-frequency characteristic and low amorphous forming ability (AFA) due to high content of Fe element [12] and low content of amorphous forming elements [13]. Recently, Fe$_{76}$Si$_{13}$B$_8$Nb$_2$Cu$_1$ nanocrystalline alloy with low H_c of 1.5 A/m, high B_s of 1.4 T, and high μ near 1.0×10^4 at 100 kHz have been successfully developed [14], showing an attractive application prospect. Nevertheless, the Fe$_{76}$Si$_{13}$B$_8$Nb$_2$Cu$_1$ alloy also needs further optimization to meet the demands of the high-frequency applications, which requires further reduction of H_c and increment of μ up to frequencies of several hundred kilohertz.

Compared with Fe-based alloys without addition of P element, the P containing FeSiBCuP [11,15] alloys had higher nanocrystallization activation energy and frequency factor which were benefit to form more uniform microstructure with high density of α-Fe (Si) grains. Accordingly, FeSiBCP [13] and FeSiPCu [16] alloys also had low H_c and high AFA. Moreover, it found that adding Mo could improve oxidation resistance, thermal stability [17–19] and high-frequency performance [20]. Besides, the addition of Mo also could improve the local packing

efficiency, inhibit grain growth, and restrain the long-range diffusion of atoms, which leading to reduction of H_c and improvement of AFA [18,21,22].

In this study, via addition of P and Mo elements, $Fe_{76}Si_{13}B_7P_1Nb_2Cu_1$ and $Fe_{76}Si_{13}B_8Nb_{1.5}Mo_{0.5}Cu_1$ nanocrystalline alloys with good soft-magnetic performances are developed. The origin of excellent magnetic softness of the FeSiBNbCu(P, Mo) alloys were discussed. Furthermore, because of the nanocrystalline soft-magnetic alloys widely used as electric devices in various magnetic field, the relations among the dynamic magnetic properties, magnetic domains, and magnetization fields on the nanocrystalline alloys are illustrated.

2. Experimental procedures

Multi-component alloys with nominal atomic compositions of $Fe_{76}Si_{13}B_7P_1Nb_2Cu_1$ and $Fe_{76}Si_{13}B_8Nb_{1.5}Mo_{0.5}Cu_1$ were prepared by induction melting with the mixtures of pure Fe (99.99 mass%), Si (99.99 mass%), B (99.9 mass%), Cu (99.99 mass%), Mo (99.9 mass%), and pre-alloy of Fe_3P under Ar atmosphere after high vacuum of about 1×10^{-2} Pa. Amorphous ribbons with width of about 1.3 mm and thickness of about 24 μm were prepared through a single-roller melt-spinning method. The thermal properties of ribbons were identified by a differential scanning calorimetry (DSC, NETZSCH 404C) at a heating rate of 0.67 °C/s. Isothermal annealing were carried out under a certain temperature from 500 to 600 °C for 10 min followed by water-quenching. In order to avoid oxidation of the samples, the annealing process was performed in a furnace with a vacuum degree of about 5×10^{-3} Pa.

The microstructures of as-quenched and annealed ribbons were investigated by an X-ray diffraction (XRD, Bruker D8 Advance) with Cu-Kα radiation and a high-resolution transmission electron microscopy (TEM, TF20). B_s was evaluated through a vibrating sample magnetometer (VSM, Lake Shore 7410) under the maximum applied field of 800 kA/m. μ was measured by an impedance analyzer (Agilent 4294 A) in AC magnetic fields from 1 to 60 A/m. H_c was conducted using a DC B-H loop tracer (EXPH-100, Riken Deshi Co., Ltd) under the maximum applied field of 800 A/m. The magnetic domain images were observed by a Magneto-optical Kerr Effect Microscopy using an Evico Magnetics Kerr Microscope (4-873K/950MT, Germany) in the longitudinal mode. The Kerr microscopy was measured on the air-bare surface of ribbon samples without further sample preparation such as polishing or coating. In order to deeply investigate the domain model and magnetization process, the changes of the domains were performed via the Magneto-optical Kerr Microscopy with in-situ applying an increasing external magnetic field with direction along the ribbon axis. The magnetic softness measurements were conducted on melt-spun or annealed ribbons with length of 75 mm. All the measurements were conducted at room temperature.

3. Results and discussion

3.1. Thermal behavior and amorphous forming ability

Thermal behavior and amorphous forming ability (AFA) were investigated after developed FeSiBNbCu(P, Mo) ribbons with good surface quality, as shown in Fig. 1. XRD measurements from 30° to 90° were performed on ribbon samples and shown in the inset (a) of Fig. 1. It can be found from the XRD patterns that P added $Fe_{76}Si_{13}B_7P_1Nb_2Cu_1$ (PA) and Mo added $Fe_{76}Si_{13}B_8Nb_{1.5}Mo_{0.5}Cu_1$ alloy (MA) ribbons prepared at a low wheel speed of 25 m/s exhibit only a halo peak at $2\theta = 45°$ corresponding to complete amorphous structure, indicating high AFA of two alloy ribbons. The DSC curves of the melt-spun basic $Fe_{76}Si_{13}B_8Nb_2Cu_1$ (BA), PA, and MA ribbons all exhibit two distinct exothermic peaks with the onset temperatures marked as T_{x1} and T_{x2} [23]. Inset Fig. 1(b) illustrates partial enlarged graph of the DSC curves. The decrease of T_{x1} for the PA and MA ribbons means easier to
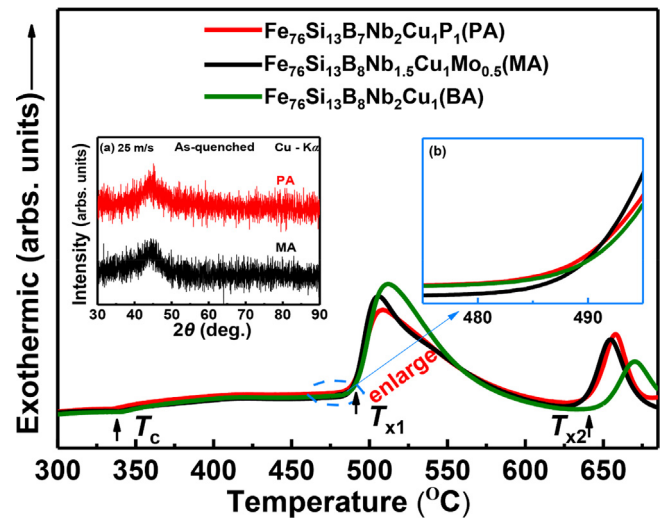
Fig. 1. DSC traces of the as-quenched $Fe_{76}Si_{13}B_8Nb_2Cu_1$ (BA), $Fe_{76}Si_{13}B_7P_1Nb_2Cu_1$ (PA), and $Fe_{76}Si_{13}B_8Nb_{1.5}Mo_{0.5}Cu_1$ (MA) ribbons. Insets: (a) XRD patterns of the as-quenched PA and MA ribbons and (b) partial enlarged graph of the DSC curves.

precipitate α-Fe (Si) phase [23]. The result is consistent with the trend of previously reported at FeSiBPCu alloy system [11,24]. It has been already reported that, in the amorphous precursor with a large $\triangle T_x$ ($\triangle T_x = T_{x2} - T_{x1}$), there is a large possibility to form single nanocrystalline α-Fe(Si) phase without precipitation of any compounds, i.e., boride by heat treatment within the annealing temperature region between the two crystallization peaks [25]. The wide temperature interval $\triangle T_x$ of PA and MA ribbons are 152 °C and 151 °C, respectively, which are slightly lower than BA ribbon but a sufficient wide temperature interval to precipitate ultrafine single nanoparticles and obtain excellent magnetic properties in the annealing process [26].

3.2. Magnetic softness dependence on annealing temperature

The magnetic properties were then investigated systematically focusing on the 10 min annealed ribbons according to optimum annealing time of BA ribbons [14]. The coercivity (H_c) dependence on annealing temperature (T_A) of annealed PA, MA, and BA ribbons exhibit similar tendency, as shown in Fig. 2(a). The H_c of both PA and MA ribbons exhibit extremely low value of 0.7 and 0.6 A/m annealed at 580 °C,
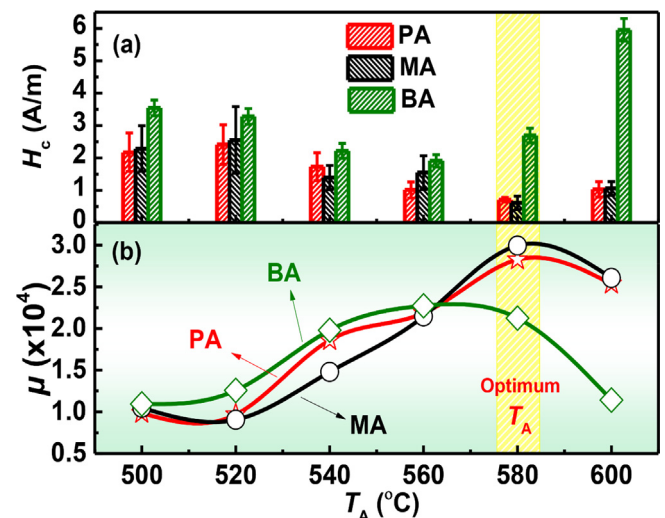
Fig. 2. Coercivity (a) and permeability (b) as a function of annealing temperature (T_A) for annealed PA, MA and BA ribbons.
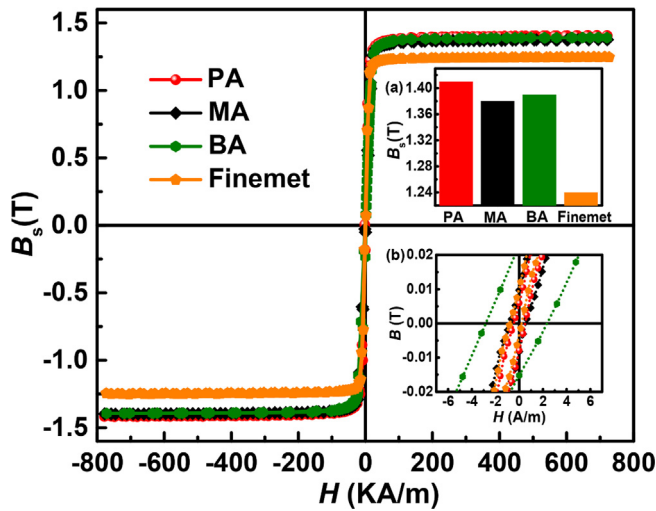
Fig. 3. Hysteresis loops of the PA, MA, BA, and Finemet ribbons after annealing at optimum conditions. Insets: (a) shows optimum B_s of four ribbons and (b) illustrates *B-H* loops measured with B-H loop tracer for optimum annealed alloys.

Table 1
Thermal behavior and magnetic softness parameters of three nanocrystalline alloys.

system	T_c (°C)	T_{x1} (°C)	T_{x2} (°C)	$\triangle T_x$ (°C)	H_c (A/m)	μ_e (1 kHz)	B_s (T)
PA	332	490	642	152	0.7	28,300	1.41
MA	338	487	638	151	0.6	30,000	1.38
BA	340	492	650	158	1.5	21,300	1.39

Fig. 4. (a) XRD patterns, (b-c) TEM bright field images, and (d-e) magnetic domains of the PA and MA ribbons after annealing at optimum conditions.

respectively. Fig. 2(b) presents the permeability (*μ*) as a function of T_A for the annealed PA, MA, and BA ribbons, which show the same trends. With the increase of T_A, the *μ* of ribbons moderately decreases at first, then it increases and reach a peak value. Especially, the peak values of PA and MA ribbons reach to 2.83×10^4 and 3.0×10^4 at 580 °C (henceforth designated as optimum T_A), respectively. It is noted that H_c and *μ* of PA and MA ribbons follow the rule of $\mu \propto H_c^{-1}$. The relations between H_c and *μ* are also existed in the many amorphous and nanocrystalline alloys [27]. The addition of P or Mo to the BA alloy could effectively improve *μ* and greatly reduce H_c. Furthermore, compared with commercial nanocrystalline Finemet alloys [3], the PA and MA ribbons are expected to have more advantages in the future applied field.

The hysteresis loops of three alloys annealed at optimum T_A were then measured with VSM. As shown in Fig. 3, all ribbons exhibit the typical loops of soft magnetic nanocrystalline alloys. It is found that the H_c of PA and MA ribbons have similar low value, which is equivalent to the H_c of Finemet alloy, as shown in inset (a) of Fig. 3. But, the B_s gains a great improvement, increase from 1.24 T for the Finemet alloy to 1.41 T for the PA alloy, as illustrated in inset (b) of Fig. 3. Similarly, compared with BA ribbons, the B_s of PA and MA ribbons have slight increase or decrease, but the H_c has been greatly optimized. It has reported that B_s is related to the ratio of the volume fraction of the crystalline phase (V_c/V) and to that of the amorphous phase (V_a/V). The B_s can be expressed as:

$$B_s = B_{sc}V_c/V + B_{sa}V_a/V \tag{1}$$

where B_{sc} and B_{sa} are the saturation magnetic flux densities of the crystalline and amorphous phases, respectively, the B_{sc} is larger than B_{sa} [28,29]. The B_s of PA ribbons is slightly higher than that of BA ribbons mainly due to easy precipitation of α-Fe (Si) phase with the additive of P element.

From the above, the specific value parameters of thermal behavior and magnetic softness of three ribbons were summarized and shown in the Table 1. It is found that the PA and MA ribbons exhibit excellent thermal behavior and magnetic properties, which is promising to be widely applied in electronics fields.

In order to obtain more convincing and detailed microstructure to prove the excellent magnetic softness of PA and MA ribbons, the XRD and TEM characterizations of the PA and MA after annealing under optimal conditions were carried out on ribbon samples, and shown in Fig. 4(a) and Fig. 4(b-c). It can be found that PA and MA ribbons both

exhibit three sharp crystalline peaks at about $2\theta = 45°$, 65°, and 83°, respectively, which can be identified as α-Fe phase from XRD patterns according to the reports [9,30]. The grain size of PA and MA ribbons were obtained with *Scherrer formula* [31] and the values are 12.8 nm and 11.6 nm, respectively. The grain size was further confirmed by TEM, the ultra-fine α-Fe nanocrystalline grains uniformly embed in the amorphous matrix and the grain sizes are 13.2 nm and 12.9 nm, respectively, which are consistent with the XRD patterns. The uniform microstructure with the fine grains is the main reason for the excellent magnetic properties of the PA and MA sample [32]. Fig. 4(d-e) show the magnetic domains of PA and MA alloy ribbons after optimum annealing. Two wide alternately bright and dark stripe domains over 70 μm with preferred orientation can be easily observed, and continuous stripe domains with alternating bright and dark could be observed in many nanocrystalline alloys after normal annealing [33–35], so sketched striped domain arrangements were shown in Fig. 4(d-e), which can directly prove that both PA and MA ribbons exhibit extremely low H_c.

3.3. Dynamic magnetization and high-frequency characterization

For the consideration of the high-frequency applications tendency of the nanocrystalline alloy, the relative permeability of the annealed
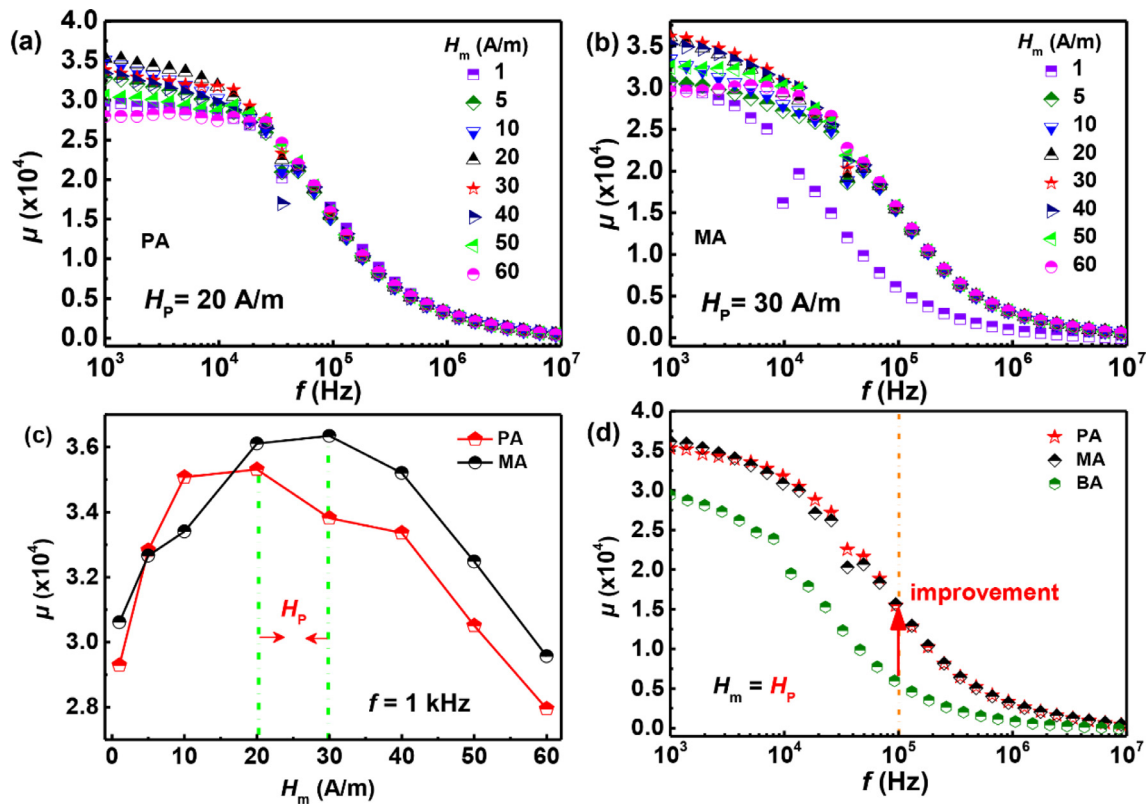
Fig. 5. (a-b) permeability spectra of the PA and MA ribbons with various applied fields at optimum annealing temperature for 10 min; (c) the changes of μ for PA and MA ribbons with H_m at 1 kHz; (d) permeability spectra of the PA, MA and BA ribbons at H_p.

ribbons under different AC magnetic field amplitude (H_m) and frequency is an important parameter [36]. The high-frequency characterization of ribbons, which were annealed at optimum condition were measured by the impedance analyzer (Agilent 4294 A) with H_m increasing. Fig. 5 (a) and (b) display the permeability spectra of the PA and MA ribbons with various applied AC fields with H_m from 1 A/m to 60 A/m at optimum annealing condition. It is found that PA and MA ribbons exhibit similar tendency with H_m increasing. All the curves are almost constant and frequency-independent in the low frequency region. As the frequency increasing, μ starts to decrease and all curves merge into one line gradually in the high frequency region. Fig. 5 (c) shows the variations of μ for PA and MA ribbons with H_m increasing measured at 1 kHz. It is clearly found that μ increases rapidly with the increase of H_m at first, and subsequently it decreases as H_m keeps increasing. The maximum μ occurs under H_m going up to a certain magnitude, and this filed magnitude is defined as pinned field (H_p) of the ribbons [33]. The maximum μ of PA and MA ribbons of 3.53×10^4 and 3.64×10^4 are obtained at H_p of 20 A/m and 30 A/m, respectively. From the Fig. 5(d), we can see that there are still relatively high μ over 1.5×10^4 at high frequency of 100 kHz, which improve a lot compared with that of the BA ribbons, indicating preferable frequency stability. The H_p of PA and MA ribbons are 20 A/m and 30 A/m, respectively, which are lower than that of other systems, such as $Fe_{82}Cu_1Si_4B_{11.5}Nb_{1.5}$ alloy and $Fe_{73.5}Si_{13.5}B_9Cu_1Nb_{3-x}Al_x$ alloys [33,37]. Lower H_p means lesser pinned sites, lesser defects and better magnetic softness [38].

At present, with the application of nanocrystalline tending to high frequency, nanocrystalline alloys are required to have higher magnetic permeability and better frequency stability at a high frequency. Compared with other high B_s nanocrystalline alloys such as FeZrB [7], FeSiBCu [10], FeSiBPCu [11] and FeSiPCu [16] alloys, PA and MA nanocrystalline alloys have huge advantage in high frequency characteristics, which will make the two alloys prospectively candidate for

various electric devices at a high frequency field.

As we know, H_p is directly related to the domain motion, and could be identified through investigating the degree of difficulties in domain movements [33,38]. The μ is also closely related to the magnetization process. Furthermore, when the investigated frequency of the ribbon is lower than the magnetic relaxation frequency, the dynamic magnetization model could be treated as a quasi-static model [39]. The relaxation frequency of PA and MA ribbons is over 100 kHz, which is wider than frequency range of this study. Therefore, the changes of domain were in-situ investigated by applied field through Magneto-optical Kerr Microscopy at 50 Hz. It can be seen from Fig. 5 that the μ of PA and MA ribbons exhibit similar tendency with applied field. Thus, we chose the optimal annealed MA ribbon to investigate the movements of domains. Fig. 6(A) shows the changes of domain width (D) and μ as a function of applied field (H) for the optimal annealed MA ribbon. It is found that both D and μ rapidly increase in a small field, then the increasing speed slow down until reaching a peak value with further increasing H. If H goes on rising, both D and μ begin to decrease. Fig. 6B (a-f) were selected from the Fig. 6A curve of the change of D, which could directly reflect the dynamic magnetization process of the optimal annealed MA ribbon. The striped domain grows fastest from graph (a) to graph (b), then it grows speed slow down from graph (b) to graph (c), then it narrows from graph (c) to graph (d), and it splits up in the graph (e), it disappears finally. Generally, when the H is lower than the H_p, the domains are pinned at original sites and only reversible and irreversible bowing occurred, which is responsible for the increase of μ [38,40]. When the H is higher than H_p, only irreversible movement such as refinement, split and reversal of domains occurred, which corresponds to μ began to decrease. Therefore, as shown in Fig. 6 A, the variation trend of μ is consistent with change of domains wall, before the value of μ reaches its maximum, the domain wall moves reversible and then irreversible. After μ reaches the maximum, the magnetic moment begins to rotate and the domain splits up and then disappears. The vanishing of
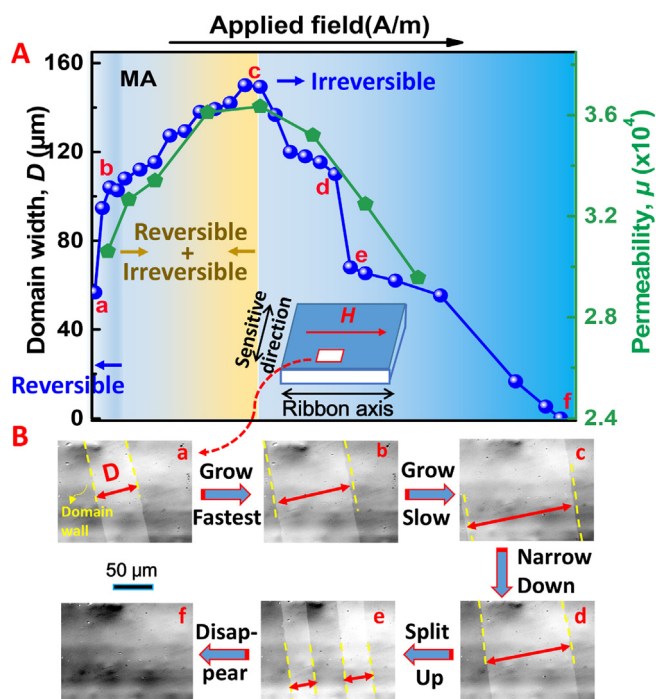
Fig. 6. A: The changes of domain width and permeability as a function of applied field for the MA ribbons; B: (a-f) Magnetic domains changes in-situ with applied field increasing.

domains means the magnetic moment reverses completely and tends to saturation, leading the μ decreases to a low value and even close to zero.

4. Conclusion

After microalloying P and Mo, the thermal behavior, magnetic softness and dynamic magnetization process of FeSiBNbCu(P,Mo) nanocrystalline alloys were investigated systematically. As a result, both $Fe_{76}Si_{13}B_7P_1Nb_2Cu_1$ (PA) and $Fe_{76}Si_{13}B_8Nb_{1.5}Mo_{0.5}Cu_1$ (MA) ribbons exhibit good thermal behavior and high AFA, together with good magnetic softness including extremely low H_c of 0.6–0.7 A/m, high μ over 3.0×10^4 and high B_s about 1.40 T. Furthermore, the P and Mo added alloys also have good high-frequency characterization, especially, the permeability at 100 kHz is still over 1.53×10^4, which will make the two nanocrystalline alloys prospectively candidate for various electric devices at a high frequency field. The excellent high frequency performance are attributed to the low pinning field and easy movement of domain walls during dynamic magnetization process due to the fine homogeneous dual-phase microstructure, and wide strip domains.

Acknowledgements

Appendix A. Supplementary data

Supplementary data to this article can be found online at https://doi.org/10.1016/j.jmmm.2019.01.116.

References

[1] G. Herzer, Modern soft magnets: amorphous and nanocrystalline materials, Acta Mater. 61 (2013) 718–734.
[2] M.E. McHenry, M.A. Willard, D.E. Laughlin, Amorphous and nanocrystalline materials for applications as soft magnets, Prog. Mater. Sci. 44 (1999) 291–433.
[3] Y. Yoshizawa, S. Oguma, K. Yamauchi, New Fe-based soft magnetic alloys composed of ultrafine grain structure, J. Appl. Phys. 64 (1988) 6044–6046.
[4] O. Gutfleisch, M.A. Willard, E. Bruck, C.H. Chen, S.G. Sankar, J.P. Liu, Magnetic materials and devices for the 21st century: stronger, lighter, and more energy efficient, Adv. Mater. 23 (2011) 821–842.
[5] O.V. Nielsen, J.R. Petersen, G. Herzer, Temperature dependence of the magnetostriction and the induced anisotropy in nanocrystalline FeCuNbSiB alloys, and their fluxgate properties, IEEE Trans. Magn. 30 (1994) 1042–1044.
[6] Y. Han, R. Wei, Z. Li, F. Li, A. Wang, C. Chang, X. Wang, Improvement of magnetic properties for V-substituted $Fe_{73.5}Si_{13.5}B_9Cu_1Nb_{3-x}V_x$ nanocrystalline alloys, J. Mater. Sci. Mater. Electron. 28 (2017) 10555–10563.
[7] A. Makino, A. Inoue, T. Masumoto, Nanocrystalline soft magnetic Fe-M-B (M = Zr, Hf, Nb), Fe-M-O (M = Zr, Hf, Rare Earth) alloys and their applications, Nanostruct. Mater. 12 (1999) 825–828.
[8] M.A. Willard, M.Q. Huang, D.E. Laughlin, M.E. McHenry, J.O. Cross, V.G. Harris, C. Franchetti, Magnetic properties of HITPERM (Fe, Co)$_{88}$Zr$_7$B$_4$Cu$_1$ magnets, J. Appl. Phys. 85 (1999) 4421–4423.
[9] X.D. Fan, B.L. Shen, Crystallization behavior and magnetic properties in High Fe content FeBCSiCu alloy system, J. Magn. Magn. Mater. 385 (2015) 277–281.
[10] M. Ohta, Y. Yoshizawa, Recent progress in high B$_s$ Fe-based nanocrystalline soft magnetic alloys, J. Phys. D: Appl. Phys. 44 (2011) 064004.
[11] A. Wang, H. Men, C. Zhao, C. Chang, R.-W. Li, X. Wang, crystallization behavior of FeSiBPCu nanocrystalline soft-magnetic alloys with high Fe content, Sci. Adv. Mater. 7 (2015) 2721–2725.
[12] X. Liang, A. He, A. Wang, J. Pang, C. Wang, C. Chang, K. Qiu, X. Wang, C.T. Liu, Fe content dependence of magnetic properties and bending ductility of FeSiBPC amorphous alloy ribbons, J. Alloy Compd. 694 (2017) 1260–1264.
[13] H.Y. Jung, S. Yi, Enhanced glass forming ability and soft magnetic properties through an optimum Nb addition to a Fe–C–Si–B–P bulk metallic glass, Intermetallics 18 (2010) 1936–1940.
[14] F. Wan, A. He, J. Zhang, J. Song, A. Wang, C. Chang, X. Wang, Development of FeSiBNbCu nanocrystalline soft magnetic alloys with high Bs and good manufacturability, J. Electron. Mater. 45 (2016) 4913–4918.
[15] A. Makino, H. Men, T. Kubota, K. Yubuta, A. Inoue, FeSiBPCu nanocrystalline soft magnetic alloys with high B$_s$ of 1.9 Tesla produced by crystallizing hetero-amorphous phase, Mater. Trans. 50 (2009) 204–209.
[16] F.G. Chen, Y.G. Wang, Investigation of glass forming ability, thermal stability and soft magnetic properties of melt-spun Fe$_{83}$P$_{16-x}$Si$_x$Cu$_1$ (x = 0, 1, 2, 3, 4, 5) alloy ribbons, J. Alloy Compd. 584 (2014) 377–380.
[17] W. Wang, Roles of minor additions in formation and properties of bulk metallic glasses, Prog. Mater Sci. 52 (2007) 540–596.
[18] W. Zhang, X. Jia, Y. Li, C. Fang, Effects of Mo addition on thermal stability and magnetic properties of a ferromagnetic Fe$_{75}$P$_{10}$C$_{10}$B$_5$ metallic glass, J. Appl. Phys. 115 (2014) 17A768.
[19] J.M. Silveyra, E. Illeková, Effects of air annealing on Fe–Si–B–M–Cu (M = Nb, Mo) alloys, J. Alloy Compd. 610 (2014) 180–183.
[20] F. Wan, T. Liu, F. Kong, A. Wang, M. Tian, J. Song, J. Zhang, C. Chang, X. Wang, Surface crystallization and magnetic properties of FeCuSiBNbMo melt-spun nanocrystalline alloys, Mater. Res. Bull. 96 (2017) 275–280.
[21] X. Jia, Y. Li, G. Xie, T. Qi, W. Zhang, Role of Mo addition on structure and magnetic properties of the Fe$_{85}$Si$_2$B$_8$P$_4$Cu$_1$ nanocrystalline alloy, J. Non-Cryst. Solids. 481 (2018) 590–593.
[22] B. Shen, M. Akiba, A. Inoue, Effects of Si and Mo additions on glass-forming in FeGaPCB bulk glassy alloys with high saturation magnetization, Phys. Rev. B. 73 (2006) 104204.
[23] K. Hono, D.H. Ping, M. Ohnuma, H. Onodera, Cu clustering and Si partitioning in the early crystallization stage of an Fe73.5Si13.5B9Nb3Cu1 Amorphous alloy, Acta Mater. 47 (1999) 997–1006.
[24] Y.Z. Makoto Matsuura, Masahiko Nishijima, Akihiro Makino, Role of P in Nanocrystallization of Fe$_{85}$Si$_2$B$_8$P$_4$Cu$_1$, IEEE Trans. Magn. 50 (2014) 1–4.
[25] H. Nam Ok, A.H. Morrish, Surface crystallization and magnetic anisotropy in amorphous Fe$_{40}$Ni$_{38}$Mo$_4$B$_{18}$ ribbons, J. Appl. Phys. 52 (1981) 1835–1837.
[26] L. Xie, T. Liu, A. He, Q. Li, Z. Gao, A. Wang, C. Chang, X. Wang, C.T. Liu, High Bs Fe-based nanocrystalline alloy with high impurity tolerance, J. Mater. Sci. 53 (2017) 1437–1446.
[27] G. Herzer, Amorphous and nanocrystalline soft magnets, Magn. Hysteres. Novel Magn. Mater. 338 (1997) 711–730.
[28] M. Ohta, Y. Yoshizawa, Cu addition effect on soft magnetic properties in Fe–Si–B alloy system, J. Appl. Phys. 103 (2008) 07E722.
[29] M. Ohta, Y. Yoshizawa, Magnetic properties of high-Bs Fe–Cu–Si–B nanocrystalline soft magnetic alloys, J. Magn. Magn. Mater. 320 (2008) e750–e753.
[30] K. Takenaka, A.D. Setyawan, P. Sharma, N. Nishiyama, A. Makino, Industrialization of nanocrystalline Fe-Si-B-P-Cu alloys for high magnetic flux density cores, J. Magn. Magn. Mater. 401 (2016) 479–483.
[31] A.L. Patterson, The Scherrer formula for x-ray particle size determination, Phys. Rev. 56 (1939) 978–982.
[32] G. Herzer, Grain size dependence of coercivity and permeability in nanocrystalline ferromagnets, IEEE Trans. Magn. 26 (1990) AQ3-AQ3.
[33] J. Zhang, F. Wan, Y. Li, J. Zheng, A. Wang, J. Song, M. Tian, A. He, C. Chang, Effect

of surface crystallization on magnetic properties of $Fe_{82}Cu_1Si_4B_{11.5}Nb_{1.5}$ nano-crystalline alloy ribbons, J. Magn. Magn. Mater. 438 (2017) 126–131.

[34] E. Lopatina, I. Soldatov, V. Budinsky, M. Marsilius, L. Schultz, G. Herzer, R. Schäfer, Surface crystallization and magnetic properties of Fe84.3Cu0.7Si4B8P3 soft magnetic ribbons, Acta Mater. 96 (2015) 10–17.

[35] P.B. Chen, A.D. Wang, C.L. Zhao, A.N. He, G. Wang, C.T. Chang, X.M. Wang, C.T. Liu, Development of soft magnetic amorphous alloys with distinctly high Fe content, Sci. China Phys. Mech. 60 (2017) 106–111.

[36] Füzer J FüzerováJ, P. Kollár, R. Bureš, M. Fáberová, Complex permeability and core loss of soft magnetic Fe-based nanocrystalline powder cores, J. Magn. Magn. Mater. 345 (2013) 77–81.

[37] H. Liu, C. Yin, X. Miao, Z. Han, D. Wang, Y. Du, Permeability spectra study of $Fe_{73.5}Si_{13.5}B_9Cu_1Nb_{3-x}Al_x$ (x = 0, 0.1, 0.2, 0.4, 0.8 and 1.6), J. Alloy Compd. 466 (2008) 246–249.

[38] C. Kittel, J.K. Galt, Ferromagnetic domain theory, Solid State Phys. 3 (1956) 437–564.

[39] L.Z. Wu, J. Ding, H.B. Jiang, C.P. Neo, L.F. Chen, C.K. Ong, High frequency complex permeability of iron particles in a nonmagnetic matrix, J. Appl. Phys. 99 (2006) 083905.

[40] Y. Ding, T. Qiu, X. Liu, Y. Long, Y. Chang, R. Ye, Permeability-frequency spectra of $(Fe_{1-x}Co_x)_{73.5}Cu_1Nb_3Si_{13.5}B_9$ nanocrystalline alloys under different magnetic fields, J. Magn. Magn. Mater. 305 (2006) 332–335.